Sensors and Actuators B 206 (2015) 190–197

Contents lists available at ScienceDirect

Sensors and Actuators B: Chemical

journal homepage: www.elsevier.com/locate/snb

Characterization of a micro-helium discharge detector for gas chromatography

Shree Narayanan [a], Gary Rice [b], Masoud Agah [a,*]

[a] VTMEMS Lab, Bradley Department of Electrical and Computer Engineering, Virginia Tech, Blacksburg, VA, USA
[b] Department of Chemistry, College of William and Mary, Williamsburg, VA, USA

ARTICLE INFO

Article history:
Received 2 April 2014
Received in revised form 20 July 2014
Accepted 6 September 2014
Available online 16 September 2014

Keywords:
Micro gas chromatography
Gas detector
Photoionization
Helium discharge

ABSTRACT

The characterization of a miniaturized helium discharge ionization detector (μHDID) for micro gas chromatography through a number of parameterized experimental measurements is presented. The response of the detector is directly related to the He discharge voltage, bias electrode-to-discharge distance, and collector-to-bias distance by a simple mathematical expression. The effect of the bias voltage and the bias and collector electrode spacings relative to the He discharge were found to improve the detector response as much as 12-fold depending on the design and various operational parameters. The detection of octane from a headspace injection was performed over 24 h of continuous operation with no noticeable degradation. Finally, a sensitivity test for octane in air was conducted using the design and parameters with the best response to obtain an absolute limit of detection of 60 pg for octane in air at 3.3 mW.

1. Introduction

Micro gas chromatography (μGC) is based on developing miniaturized, portable systems capable of identifying the composition of a gas mixture by separation into its individual components. Such analyses are highly applicable for homeland security, space exploration, on-site or distributed environmental monitoring mechanisms, food assessment, etc. [1–13]. In a typical μGC system, the sample mixture is first collected on an adsorbent bed referred to as the pre-concentrator. When thermally spiked, this device releases the adsorbed species in a sharp vaporized plug. This narrow plug enters a microfluidic channel, called the separation column, which is coated with a stationary phase film to chemically interact and retard the various analytes of the plug to different extents. The analytes are then separated in time and, ideally, elute out of the column one-by-one into a detector. The movement of the analytes through the entire system is facilitated by an inert carrier gas (mobile phase) such as helium or nitrogen.

Miniaturization offers unique advantages such as light-weight, low power consumption, less reagent usage and innovative architectures apart from lower cost when batch fabricated [14–27]. Stereotypical miniaturization utilizes components fabricated in silicon/glass. Common implementations involve etching a narrow bore microfluidic channel in silicon/glass wafers, with capillary dimensions similar to conventional GC columns, or fabricating posts within the silicon cavity and coating with an adsorbent material. The primary incentive is the ability to conveniently pack a 1–2 m length tubing (cavity) into a 2 cm × 4 cm × 500 μm silicon die without having to wind equivalent length capillary tubing into a large coil. In addition, heating a silicon die with on-chip heaters is energetically far less taxing compared to heating capillary tubing with a convection oven.

The choices for detectors in the micro-world are numerous. While traditional GC systems are dominated by flame ionization detectors (FID), electron capture detectors (ECD) and flame photometric detectors (FPD), μGC offers the possibility of obtaining signals via other forms of reactive processes using sorptive sensors that transduce into electrical, acoustic or optical domains [28–34]. In general, any concentration-sensitive detector, such as the thermal conductivity detector (TCD), is more pliable to be reduced in size [35,36]. It should be noted that while ionization detectors such as the FID provide robust performance and sensitivity, efforts to miniaturize them do not yield comparable detection levels since the hydrogen flame loses its ionizing potential when reduced in size [37,38]. On the other hand, sorptive and thermal sensing detectors have inherent limitations since they are more temperature sensitive and hence their implementation and application has been inadequate as well. Mass spectrometry (MS), considered the gold standard in conventional analytical techniques, has also been subject to miniaturization. A majority of these efforts has focused on reducing the size of a MS using techniques that are not found in silicon micromachining. This has resulted in dimensions slightly

* Corresponding author. Tel.: +1 5402312653.
E-mail address: agah@vt.edu (M. Agah).

http://dx.doi.org/10.1016/j.snb.2014.09.014
0925-4005/

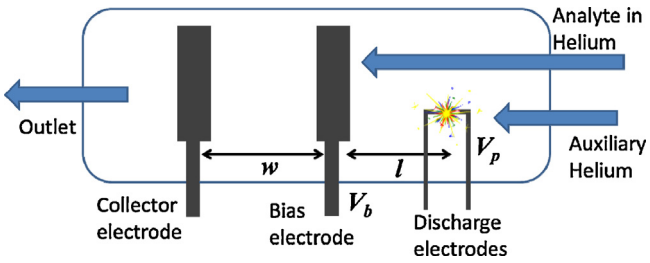

Fig. 1. A schematic diagram showing the dual-inlet, single-outlet μHDID. The analytes from a micromachined separation column are introduced at the top of the bias electrode, bypassing the auxiliary channel fed helium microdischarge. Ionization of analytes in the region between the collector and bias electrodes results in the detector response at the collector electrode. The parameters of interest, namely l, w, V_p, and V_b are denoted.

larger than that found in microGC and a power dissipation on the order of tens of watts [39].

Commercially available μGC systems have adopted a hybrid approach wherein the detector is similar in style to conventional ultraviolet photoionization detectors (UV-PID). These systems offer excellent detection sensitivity, but are somewhat restricted by the photoionization energies available (<11.7 eV with argon lamps) as well as incorporation into a μGC system. Micro-discharges or plasmas have also been utilized in gas detectors since 1991. Eijkel et al. reported on a detector for μGC that fragmented the analytes in a DC microplasma to produce diatomic fragments from which emission was detected spectrophotometrically [40]. Improvements on this technique included an innovative electrode structure to generate a pulsed plasma with drastically reduced power consumption [41,42]. Spectrophotometric detection is an intensive operation that can consume power on the order of watts. An alternative is to monitor the current through the discharge itself as reported by Fu et al. [43]. However, a common concern with these designs is the fouling of the electrodes due to fragmentation of the analytes. Fragmentation also does not allow for the analytes to be subjected to further analysis.

We previously reported on a proof-of-concept micro-helium discharge detector [44] to address the need for a sensitive, low-power, easy-to-fabricate universal detector. This microdischarge utilizes high-energy photons and excited state helium metastable species to ionize the analytes and the resultant current monitored on a remote collector electrode. Their lack of sensitivity to temperature makes them suitable for robust gas detection systems [45]. A limit of detection (LOD) of 350 pg for octane was demonstrated. Additional design parameters for our μHDID are considered here. Specifically, the effect of the He discharge voltage, distance of the bias electrode from the He discharge, collector electrode from bias electrode, and the bias voltage are parametrically studied. The results were used to choose the best design to enhance the LOD.

2. Theory

The micro-helium discharge ionization detector (μHDID) is an ionization style detector that operates by measuring the resultant current from ionization of the analytes without molecular fragmentation (Fig. 1). It utilizes a high voltage DC discharge in helium across a 20 μm gap as the source of high energy photons and metastable excited helium atoms, which are thought to be the dominant species responsible for the ionization of analyte species. This is partly inspired by a pulsed discharge helium ionization detector that utilizes a pulsing technique to arc across an electrode pair to generate the excitation source [46,47]. Fig. 1 is a schematic showing the concept and design parameters of the detector. Apart from the discharge electrode pair to produce the He micro-discharge, the device also consists of a bias electrode and a remote collector electrode downstream from the microplasma. Analytes contained in a helium carrier from the separation column are introduced into the detector at the bias electrode. The space between the bias and collector electrode defines the "volume of the collector" and dictates to some extent the level of signal response generated.

When suitably excited, the He discharge results in the generation of a complex mix of positive and negatively charged ions, metastable He atoms, electrons, and photons. These omnidirectional energetic particles constitute what is called the ionizing flux. Some of these particles, such as metastable helium atoms and ions, flow downstream due to pressure-driven flow. Thus, the ionizing flux at the bias electrode is a mix of positive and negatively charged particles as well as high energy photons and metastable He atoms. The high energy components of this ionizing flux (normally considered to be photons with energies >10 eV and metastable He atoms with energies of 19.8 eV) are responsible for ionization of analyte species eluting from the GC column. The transmission of this flux through the detector volume decays exponentially due to absorption, and is given by

$$I_b = I_0 e^{-\alpha l} \quad (1)$$

I_b, the flux observed at the bias electrode is related to the initial discharge emission I_0 by Beer–Lambert's law for photon flux transmission. α is the absorption coefficient of helium over the length of the detector (l) from the He discharge to the bias electrode. One can rationalize that l should be minimized to increase the flux density available at the bias electrode. On a similar note, the gap width w should be maximized to increase the total flux available for the analyte species within the collector volume where the photon flux needs to be absorbed to the maximum extent. However, recombination processes with electrons within this volume can cause a portion of the generated carriers to be neutralized and hence not detected. The net effect of these factors determines the distance from the collector electrode in which a generated charge carrier will result in a favorable current. In the presence of a bias voltage, the effect of an electric field between closely spaced bias and collector electrodes can be advantageous in isolating the generated carriers within the collector volume more efficiently. The lifetime of metastable He species available for collisional energy transfer to analyte species will be a factor as well. A number of these factors are considered in the following discussions.

3. Experimental

3.1. Materials and sample preparation

Borosilicate glass wafers (Borofloat 33, Schott, NY) of 700 μm thickness and 100 mm diameter were used as substrate wafers for fabrication of the microplasma devices. The separation columns were prepared from 100 mm $\langle 100 \rangle$ silicon wafers (Test grade, University Wafers, MA) of 500 μm thickness.

For the design characterization experiments, the headspace of a 1.8 mL autosampler vial filled with about 120 μL of reagent grade n-octane served as the source for constant vapor phase concentrations for gas-phase injections. For the limit-of-detection (LOD) experiments, 25–200 μL of analytical grade n-octane were pipetted into a custom-made 1 L volumetric flask. The mouth of the flask was sealed with a 24/40 septa and left overnight for the octane to volatilize. To prepare a different dilution, the octane in the flask was cleared by removing the septa seal and running the flask through a cycle of nitrogen purging, oven heating at 80 °C, and repurging with nitrogen. After letting the flask cool down to room temperature, the volume of octane corresponding to the desired concentration

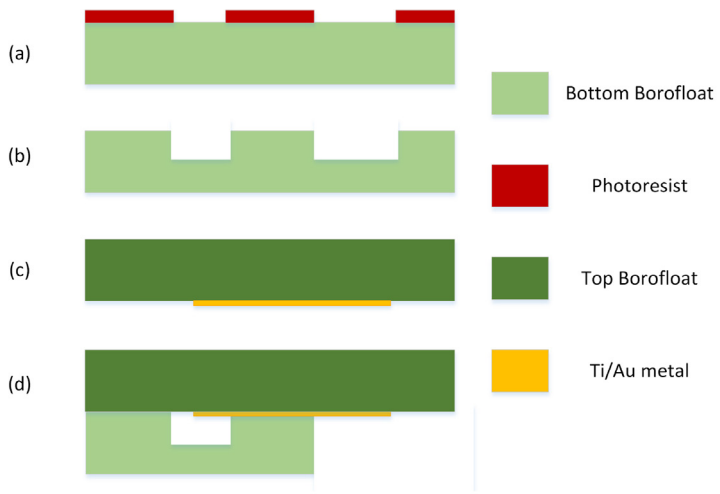

(i)

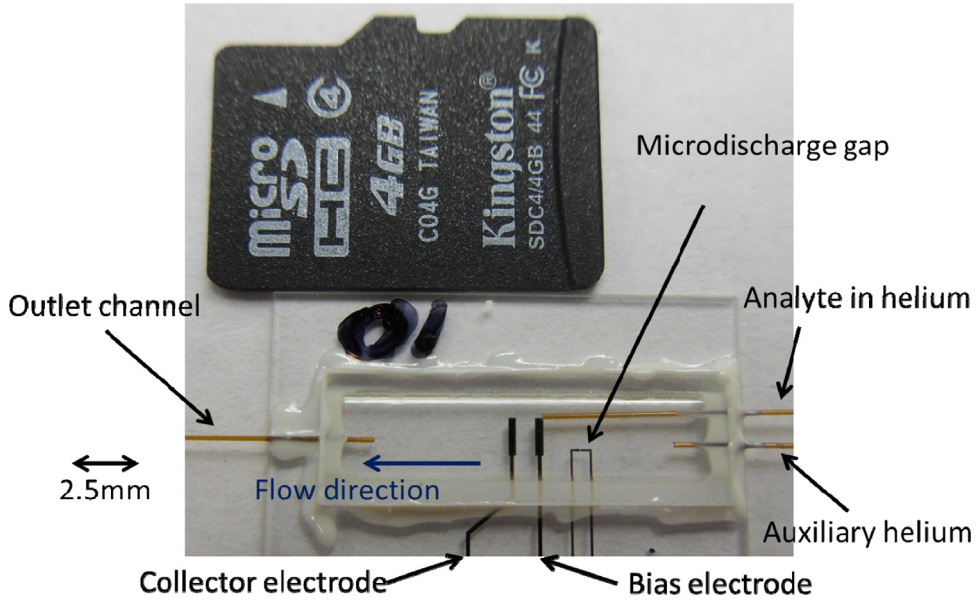

(ii)

Fig. 2. (i) Top image shows the fabrication of the detector using Borofloat wafers. The top bottom wafer is patterned in (a), and wet etched and stripped in (b) to obtain the microfluidic channels. In (c) a lift-off on top wafer deposits the patterned metal structures for the electrodes. The wafers are diced and epoxy-bonded in (d). An optical image of the μHDID right next to a micro-SDcard is shown at the bottom in (ii).

was pipetted into the flask, which was then re-sealed and left to homogenize.

3.2. Fabrication

The detector was constructed from two Borofloat wafers. To fabricate the microfluidic channels, a (bottom) Borofloat wafer was blanket deposited with 50 nm/30 nm chromium/gold by e-beam physical vapor deposition (PVD-250, Kurt Lesker). Photoresist (AZ9260) was spun-coated and lithographically patterned with the first mask that exposes an area corresponding to the fluidic channels and bond pads. After etching the chromium and gold layers, the Borofloat was deep etched to a depth of 260 μm using a 10:1 HF/HCl mixture (Fig. 2(a)). Following this, the mask was completely stripped off. The top Borofloat wafer was spun-coated with AZ9260 and patterned. A 1 μm/25 nm titanium/gold stack was e-beam deposited and patterned by lift-off. Both the wafers were diced into individual devices and bonded together with epoxy (Fig. 2(d)). Capillary tubing of 100 μm I.D. and 200 μm O.D. (Polymicro TSP100200) were slid into the channel exits and sealed with a two-part epoxy (Epoxy 907, Miller Stephenson, Danbury, CT). A picture of the completed assembly is shown in Fig. 2(ii). An 80 μm-wide, 240 μm-deep and 1 m-long micromachined separation column was fabricated using a standard process described elsewhere [44] for the octane separations. Polydimethylsiloxane (OV-1, Ohio Valley, OH) was used as the stationary phase to static coat the separation column [48].

A listing of the devices compared and their design parameters are provided in Table 1, and illustrated in Fig. 1. Devices within design parameter sets 1–3 were fabricated with a fixed bias to collector–electrode distance (w = 2.5 mm) but vary with the distance of the bias electrode from the He discharge (l). Devices within

Table 1
Six different designs with values for the parameters l (distance between the He discharge and bias electrode) and w (distance between the bias and collector electrode). The distance from He discharge to the midpoint of the gap between the electrodes is calculated in the fourth column from the previous two. Multiple devices of the same design were tested in most cases.

Design #	Length l (mm)	Gap width w (mm)	Discharge to gap midpoint $(l+w/2)$ (mm)
1	5	2.5	6.25
2	3	2.5	4.25
3	1.5	2.5	2.75
4	1.5	1	2
5	1.5	2	2.5
6	1.5	3	3

design parameter sets 4–6 have the bias electrode at a fixed distance from the He discharge (l = 1.5 mm) but vary in the distance of the collector from the bias (w). The third column provides the distance from the midpoint between the collector and bias electrodes to the He discharge. Its significance will be discussed in a later section.

3.3. Measurement setup

A GC oven (Model 7890, Agilent, Santa Clara, CA), fitted with two electronic pressure control (EPC) inlets and an FID was used to test the detector, as shown in Fig. 3. A G4513A autosampler was fixed to Inlet A of the GC when automated injections were required. The automated injection was configured for two sample priming events followed by drawing 1 μl from the 1.8 mL autosampler vials, all at a depth of 10 mm, to ensure consistent gas phase injections. A gas tight syringe (Catalog number 80000, Hamilton Syringe Company, Reno, NV) was used for making manual injections of samples during LOD testing. Ultra high purity helium (UHP 300, Airgas) was used as the carrier and auxiliary gases. Industrial grade air (AIB 300, Airgas) and hydrogen generated by a hydrogen generator (Model 20H, Domnick Hunter) provided the FID gas supplies. One end of the separation column was connected to Inlet A of the GC held at 96.5 kPa. The split flow on this inlet was set to allow 1/150 of the sample volume injected to reach the column. The other end of the column was connected to the analyte channel of the detector. The analyte channel bypassed the He discharge, which was fed by a helium flow from Inlet B of the GC at 27.6 kPa, resulting in a 0.22 mL/min flow rate through the auxiliary channel. Both injection inlets and the FID were maintained at 280 °C whereas the μHDID was maintained at ambient temperature. A picoammeter (Model 480, Keithley, Cleveland, OH) was used to detect the signal from the remote electrode while a LabVIEW (National Instruments, Austin, TX) program recorded the measurement from the rear-terminal output viz. a digital multimeter (Model 2700, Keithley, Cleveland, OH). High voltage power supplies (PS310, Stanford Research Systems, Sunnyvale, CA) were used to provide the voltage necessary for the He discharge as well as the bias electrode voltage.

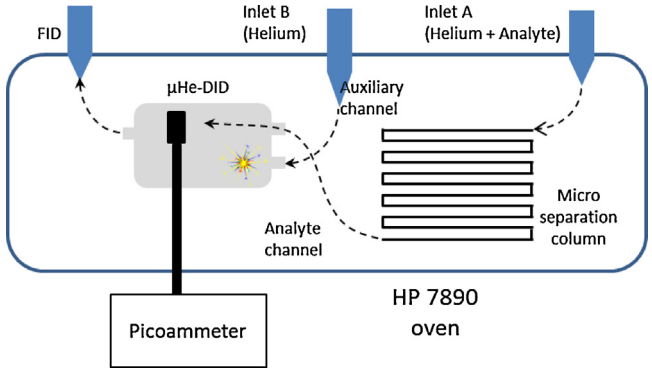

Fig. 3. A setup showing the connections of the He-DID. The auxiliary channel feeds helium for the microdischarge. The analyte channel introduces the analytes from the separation column, bypassing the microdischarge. The picoammeter reads of the signal from the remote electrode. The FID is used only for verifying the consistency of the injection.

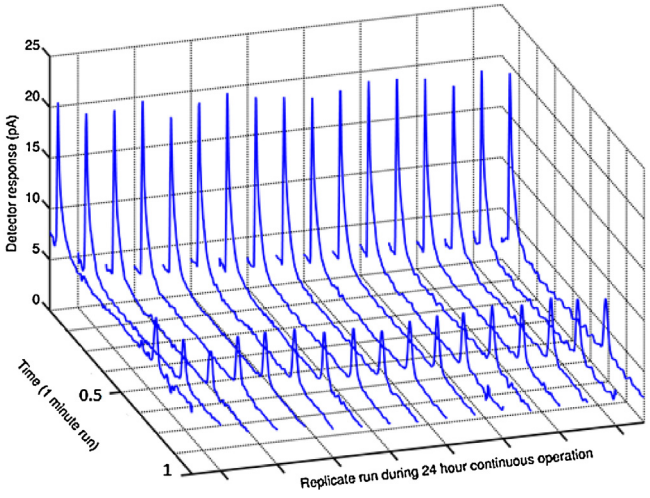

Fig. 4. A series of chromatographic runs from injections of octane vapor in an autosampler vial headspace as detected by the μHDID. Chromatograms were taken regularly during a 24 h continuous operation, with the earliest to the left. Each 5-point moving average shows two prominent peaks – a very early large peak due to air and a small late peak due to octane.

4. Results and discussion

4.1. Long term operation

The packaged detector was setup as shown in Fig. 3. A 550 V DC potential was applied through a 50 MΩ resistor, across the discharge electrodes with the bias electrode grounded, and the current from the collector electrode recorded through the picoammeter. In order to study the empirical impacts of the signals generated over long time intervals, a 1 μL headspace of octane was injected from an autosampler every 1.5 h over 24 h of continuous operation and the response of the detector (via the picoammeter) recorded. Fig. 4 shows a stacked plot of the recordings with the earliest recording to the left. The raw data was smoothed with a 5-point moving average. The first peak corresponds to air, while the smaller peak that elutes at about 0.7 min corresponds to octane. The baseline for the detector decreases from its initial value by about 50% to eventually stabilize within 4 h (as shown in Fig. 5). This "burn-in" period was noticed in the first few hours of every detector and could correspond to the sputtering off of gold from the electrodes used to produce the discharge as well as removal of contaminant compounds used in the fabrication process. The burn-in process is not required every time the detector is operated, it is only necessary after initial fabrication of the detector. Thereafter, the baseline was observed to be relatively stable and the detector's response (peak height minus baseline) considered reasonably constant for measurements.

4.2. Distance of the bias electrode from the discharge (l)

Multiple detectors of three different designs (Designs 1–3 in Table 1) were fabricated with a fixed distance between the bias and collector electrodes at 2.5 mm, and varying distances between the bias electrode and the He discharge. A total of 6 different detectors were tested (two of each of the three designs). The response of the detectors to 1 μL injections of octane in the headspace of

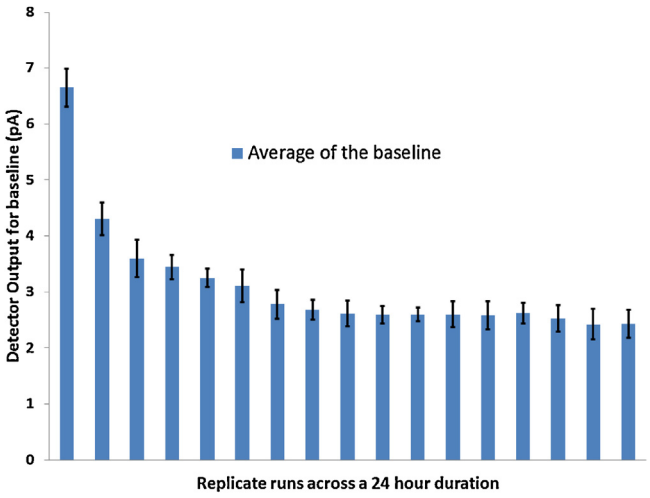

Fig. 5. Plot of the average baseline obtained over a 24 h period with the error bars indicating the variation in the baseline (noise) for each chromatographic run.

autosampler vials was measured with excitation voltages from 550 V to 700 V in increments of 50 V used to produce the He discharge, with the bias electrode grounded. The peak height corresponding to octane for the range of discharge voltages is plotted in Fig. 6 for each design. Three tests were performed at every voltage for each of the 6 detectors, two of each design, and the peak heights averaged. The error bar represents the standard deviation in the multiple measurements. The positive slope on each line plot indicates that an increased voltage (V_p) predictably results in an enhanced response. This can be correlated to a larger current flux within the discharge gap, which produces a larger ionizing flux. This would be reflected in an increase in the value of I_0 in Eq. (1). Deviations from monotonicity were matched to variations in the sample injected by the autosampler itself, as observed for signals obtained from the FID (data not shown here).

The octane signal was also observed to increase significantly in Fig. 6 for smaller values of l. As the distance between the He discharge and the bias electrode is decreased, the flux observed at the bias electrode increases. This effect can be correlated to the exponential term in Eq. (1), and correspondingly results in better

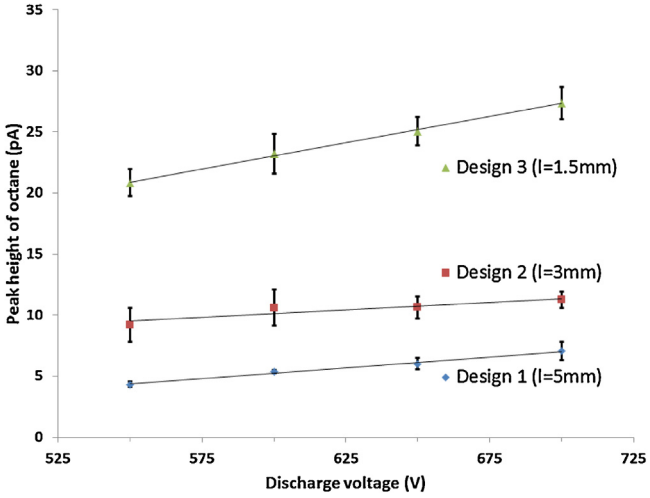

Fig. 6. Variation in the detector response to octane headspace injection at different discharge voltages for 3 designs (6 different devices). The devices are characterized by the distance from discharge to bias electrode (l) with a constant w = 2.5 mm. Each data point is the average over multiple runs.

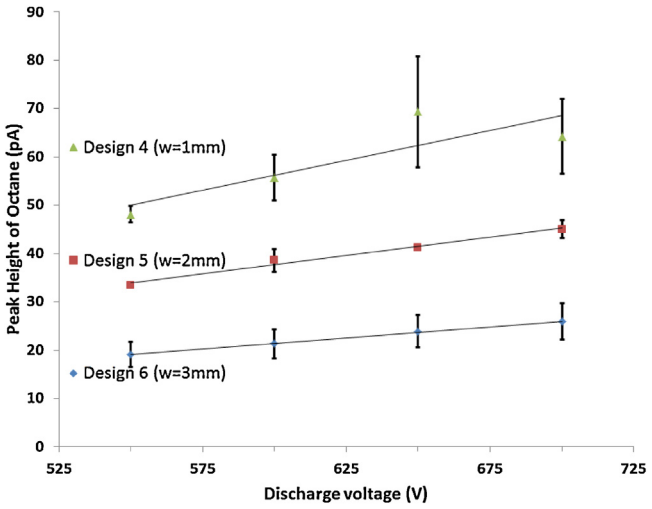

Fig. 7. Variation in the detector response to octane headspace injection at different discharge voltages for five different devices with variations in the bias to collector electrode distance (w) with a constant l = 1.5 mm. Each data point is the average from multiple runs.

analyte ionization. In addition, the number of high energy photons and metastable He atoms available for analyte ionization should be enhanced by reducing the distance between the discharge and the capillary outlet directly above the bias electrode, effectively improving the density of the ionizing flux at the capillary outlet. Thus, it can be concluded that for a given w, the detector with the smallest value for l gives a better response. The extent to which l can be minimized is limited by the possibility of fragmentation of the analyte upon their introduction at the bias electrode and subsequent back-diffusion. This limitation has not been explored in this paper and is subject to further investigation.

4.3. Distance of the collector from the bias electrode (w)

Multiple detectors of three different designs (Designs 4–6) were fabricated and tested with the location of the bias electrode from the He discharge set at 1.5 mm. However, the distance of the collector electrode from the bias electrode was varied to understand the competing effects of ionization and recombination within the collector volume. Plots for the detector response for three designs over the same range of discharge voltages are shown in Fig. 7. Each data point is the average of triplicate runs performed on each detector at each voltage, from a total of 5 detectors. The error bars represent the standard deviation of the values for which the average is plotted. In a manner similar to the distance between the bias electrode and He discharge, signals were observed to increase as the distance between the collector and bias electrodes decreased. The signal collected at the collector electrode relies on the ionization of analytes from the He discharge source to produce charged species with a sufficient lifetime to reach the collector electrode via the helium flow through the device. As this gap decreases, the time available for recombination effects, or neutralization of the charged species, decreases as well. Thus, for a given l, decreasing the width w is favorable. The reason for the decrease in signal observed at the highest discharge voltage for Design 4 is unclear at this time.

The results from the previous two experiments can be combined to obtain a simple relation for the detector response R (peak height of the octane signal) in terms of the length l and width w,

$$R \propto V_p e^{-\alpha l}(1 - \beta w) \quad (2)$$

Here, α is the absorption coefficient from Beer–Lambert's law. β is an empirical coefficient to account for the improved

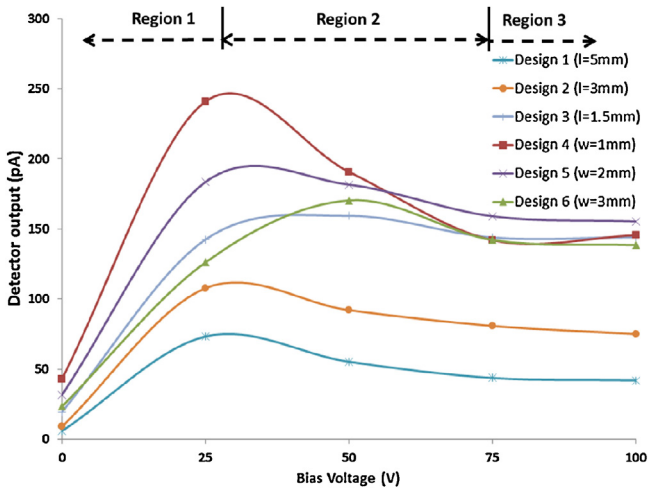

Fig. 8. Response of the detector to octane headspace injections from stepped values of bias voltage from 0 to 100 V. Each data point is the average from two runs. A detector from each previously tested design was used for this analysis.

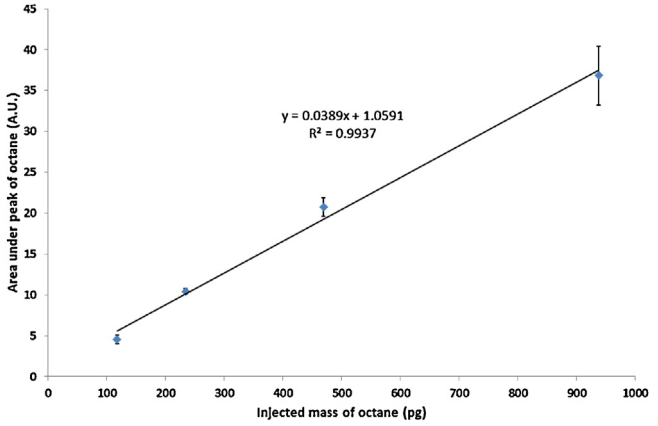

Fig. 9. Response of the chip (Design 4) to various injected masses of octane, at a bias voltage of 25 V. Each data point is the average from three successive runs.

collection as the collector is brought closer to the bias electrode and can be related to the presence of a first order recombination/decay length constant. Using the slopes generated from the data plotted in Figs. 6 and 7, the values of α and β were estimated to be 0.45 mm^{-1} and 0.23 mm^{-1}, respectively, at 550 V. The larger the value of α, the quicker the decay of the flux from the He discharge and hence, the closer the bias electrode has to be positioned to the He discharge. On the other hand, a lower value of β makes the design less sensitive to the width of the gap (w).

4.4. Bias voltage, V_b

The role of bias voltage in actively collecting charged species within the collector volume was examined by stepping the voltage from 0 to 100 V in increments of 25 V and measuring the detector response. Fig. 8 also presents the effect of the electrode parameters on the detector response in the presence of a stepped bias voltage. A detector from each previously tested design was tested with the He discharge voltage (V_p) set to 550 V. Each data point is the average of two runs. One run was obtained while stepping the voltage up from 0 to 100 V and the other stepping down from 100 to 0 V.

The plot in Fig. 8 can be split into three regions and the behavior of the detector hypothesized as follows. The analytes within the collector volume can be readily ionized by high energy photons and metastable He species from the ionizing flux. In Region 1, in the presence of a small positive bias, negatively charged species from the ionizing flux are collected at the bias electrode, which effectively reduces the possibility of recombination with the positive ions produced from the analytes. Similarly, the electrons created by the soft-ionization of the analytes within the collector volume are collected as well; in effect increasing the time necessary for recombination of the electrons with the ionized analytes. The resultant effect is signal amplification, as noted with the increase in detector output. The sensed current is thus a sum of the effect of the increase in the drift current owing to the removal of the negative species within the volume, and the secondary emission from the impinging flux on the bias. While the former depends on the proximity of the collector electrode to the bias electrode, the latter depends on the proximity of the bias electrode to the He discharge. The slope of the graph, in this region, can be related to the parameter ($l + w/2$), previously described as the distance of the midpoint of the gap from the He discharge, and tabulated in Table 1.

Beyond a certain voltage, the impact of the bias electrode on repelling positively charged species in the ionizing flux and the collection of high energy electrons reduces the ionization detected within the collector volume. This results in a decrease in detector response, as observed in Region 2 that eventually levels off into Region 3. If one assumes that a significant fraction of the ionized analyte species is the result of metastable He atoms, then this implies that above a certain threshold voltage that energetic primary and secondary electrons responsible for the production of some of the metastable He population are depleted by the bias electrode. This would leave high energy photons produced in the ionizing flux as the primary means of analyte ionization, essentially resulting in a saturated signal since the photon population would be primarily dependent on the He discharge voltage and not the bias voltage. Since the ionizing flux depends only on the proximity of the bias electrode to the He discharge, the saturated response increases with decreasing values of l but is not affected by w since removal of the electron population significantly reduces the detrimental impact of recombination with analyte ions. This is experimentally evident from the similar detector outputs observed in the saturated region (III) for Designs 3–6 with the same value of $l = 1.5$ but varying in w. Measurements were taken with finer resolution in bias voltages between 0 and 50 V. While, the data fit the overall trend of the plot, a relation between the exact voltages of peak response could not be established due to measurement variations associated with such fine voltage resolution measurements.

4.5. Limit of detection (LOD)

A sensitivity test for the device with the best response (Design 4 in the bias voltage experiment) was performed using various dilutions of octane vapor in air. 1 μL samples from mixtures of 25, 50, 100 and 200 μL of octane in 1 L of air were drawn into a gas tight syringe and injected into Inlet A of the GC. The discharge voltage was set to 700 V and the bias to 25 V. The power consumption was calculated to be 3.3 mW under these conditions. A calibration curve plotting octane peak area against the injected mass in Fig. 9 exhibited some deviation from linearity at the highest octane mass (950 pg). The worst case deviation in baseline noise from all 9 runs was 2.5 pA. Using a 3/1 signal to noise ratio as the criteria for the absolute limit of detection and plugging into the quadratic fit, an LOD of 60 pg for octane was obtained.

5. Conclusions

This paper reported on the optimization of a miniaturized He discharge ionization detector for micro gas chromatography. Specifically, the placement of the bias from the discharge, and the gap between the bias and collector electrodes was studied. It was

observed that while the bias electrode's distance had an exponential effect, the gap between the bias and collector electrodes had a linear effect. In addition, the plasma voltage was found to have a proportional increase in the detector's response due to increase in the ionizing flux. On the other hand, there is an optimal bias voltage that provides maximum increase in the output due to the complex interaction mechanism. Preliminary results indicate that column temperature has negligible effect on the detector response. An improved detection limit of 60 pg was reported.

Detector response to other compound classes such as aromatics and halogenated species should be investigated as well since ionization potentials can vary depending on the compound structures. In addition, the role of flow rate from both the analyte and auxiliary channels need to be better understood and optimized to further improve the signal-to-noise ratio (SNR). Further research efforts will ultimately lead to the integration of the detector with the separation column for an integrated portable analysis system.

Acknowledgements

The authors would like to thank Mr. Don Leber with the Virginia Tech MicrOn cleanroom for his technical assistance. The authors would also like to acknowledge the funding sources: National Science Foundation CAREER award (ECCS-0747600) and NIOSH grant (5R21OH010330).

Appendix A. Supplementary data

Supplementary data associated with this article can be found, in the online version, at http://dx.doi.org/10.1016/j.snb.2014.09.014.

References

[1] G. Monti, et al., Monitoring food quality by microfluidic electrophoresis, gas chromatography, and mass spectrometry techniques: effects of aquaculture on the sea bass (*Dicentrarchus labrax*), Anal. Chem. 77 (8) (2005) 2587–2594.
[2] D. Puente, et al., Thermal conductivity microsensor for determining the methane number of natural gas, Sens. Actuators B: Chem. 110 (2) (2005) 181–189.
[3] R.W. Cernosek, et al., Micro-analytical systems for national security applications, in: Proc. SPIE-Micro (MEMS) and Nanotechnologies for Space Applications, Orlando (Kissimmee), FL, USA, 2006, p. 622306.
[4] D. Nielsen, Practical Handbook of Environmental Site Characterization and Ground-water Monitoring, CRC press, Boca Raton, FL, 2006.
[5] A.D. Radadia, et al., Micromachined GC columns for fast separation of organophosphonate and organosulfur compounds, Anal. Chem. 80 (11) (2008) 4087–4094.
[6] B. Alfeeli, et al., MEMS-based selective preconcentration of trace level breath analytes, IEEE Sens. J. 9 (9) (2009).
[7] M. Akbar, et al., A microfabricated propofol trap for breath-based anesthesia depth monitoring, J. Microelectromech. Syst. 99 (2012) 1–9.
[8] H. Shakeel, et al., First reconfigurable MEMS separation columns for micro gas chromatography, in: 2012 IEEE 25th International Conference on Micro Electro Mechanical Systems (MEMS), 2012, pp. 823–826.
[9] S.K. Kim, et al., Microfabricated gas chromatograph for the selective determination of trichloroethylene vapor at sub-parts-per-billion concentrations in complex mixtures, Anal. Chem. 83 (18) (2011) 7198–7206.
[10] I. Elmi, et al., A miniaturized gas-chromatographic system for the evaluation of fish freshness, in: IEEE Sensors, 2008, pp. 1084–1087.
[11] R.R. Reston, et al., Silicon-micromachined gas chromatography system used to separate and detect ammonia and nitrogen dioxide. I. Design, fabrication, and integration of the gas chromatography system, J. Microelectromech. Syst. 3 (4) (1994) 134–146.
[12] D. Wang, et al., Highly stable surface functionalization of microgas chromatography columns using layer-by-layer self-assembly of silica nanoparticles, Anal. Chem. July (2013) (Epub ahead of print).
[13] H. Shakeel, et al., Self-patterned gold-electroplated multicapillary gas separation columns with MPG stationary phases, J. Microelectromech. Syst. 22 (February (1)) (2013) 62–70.
[14] S.C. Terry, et al., A gas chromatographic air analyzer fabricated on a silicon wafer, IEEE Trans. Electron Devices 26 (12) (1979) 1880–1886.
[15] S. Showalter, et al., Design and Testing of a Micro Thermal Conductivity Detector (TCD) System, SAND2003-0954, Sandia National Labs, Albuquerque, NM, USA, 2003.
[16] R. Manginell, et al., Advancements in the Monolithically-Integrated MicroChemLab, in: Proceedings of the m-TAS 2004 Workshop, Malmo, Sweden, 2004, pp. 61–63.
[17] G. Lambertus, et al., Stop-flow programmable selectivity with a dual-column ensemble of microfabricated etched silicon columns and air as carrier gas, Anal. Chem. 77 (7) (2005) 2078–2084.
[18] S. Ali, et al., MEMS-based semi-packed gas chromatography columns, Sens. Actuators B: Chem. 141 (1) (2009) 309–315.
[19] C.-J. Lu, et al., First-generation hybrid MEMS gas chromatograph, Lab Chip 5 (10) (2005) 1123–1131.
[20] M. Agah, et al., Low-mass PECVD oxynitride gas chromatographic columns, J. Microelectromech. Syst. 16 (4) (2007) 853–860.
[21] J.J. Whiting, et al., High-speed two-dimensional gas chromatography using microfabricated GC columns combined with nanoelectromechanical mass sensors, Transducers (2009) 1666–1669.
[22] J. Liu, et al., Adaptive two-dimensional microgas chromatography, Anal. Chem. 84 (9) (2012) 4214–4220.
[23] R. Manginell, et al., A monolithically-integrated μGC chemical sensor system, Sensors 11 (7) (2011) 6517–6532.
[24] B. Alfeeli, et al., MEMS-based multi-inlet/outlet preconcentrator coated by inkjet printing of polymer adsorbents, Sens. Actuators B: Chem. 133 (1) (2008) 24–32.
[25] B. Byunghoon, et al., A fully-integrated MEMS preconcentrator for rapid gas sampling, in: Solid-State Sensors, Actuators and Microsystems Conference, 2007. TRANSDUCERS 2007, 2007, pp. 1497–1500.
[26] R.P. Manginell, et al., Mass-sensitive microfabricated chemical preconcentrator, J. Microelectromech. Syst. 17 (6) (2008) 1396–1407.
[27] C.-J. Lu, et al., A dual-adsorbent preconcentrator for a portable indoor-VOC microsensor system, Anal. Chem. 73 (14) (2001) 3449–3457 (01.07.01).
[28] S.J. Martin, et al., Gas sensing with acoustic devices, in: Ultrasonics Symposium, 1996. Proceedings, 1996 IEEE, vol. 1, 1996, pp. 423–434.
[29] M. Kimura, et al., Application of the air-bridge microheater to gas detection, Sens. Actuators B: Chem. 25 (1–3) (1995) 857–860.
[30] L.K. Wright, et al., A nanoparticle-coated chemiresistor array as a microscale gas chromatograph detector for explosive marker compounds: flow rate and temperature effects, Analyst 138 (22) (2013) 6860–6868.
[31] I. Simon, et al., Micromachined metal oxide gas sensors: opportunities to improve sensor performance, Sens. Actuators B: Chem. 73 (1) (2001) 1–26.
[32] Q.-Y. Cai, et al., Dual-chemiresistor GC detector employing monolayer-protected metal nanocluster interfaces, Anal. Chem. 74 (14) (2002) 3533–3539.
[33] S. Bedair, et al., CMOS MEMS oscillator for gas chemical detection, in: Proceedings of IEEE Sensors, 2004, pp. 955–958.
[34] K. Reddy, et al., On-chip Fabry–Pérot interferometric sensors for micro-gas chromatography detection, Sens. Actuators B: Chem. 159 (1) (2011) 60–65.
[35] R. Pecsar, et al., Performance of a reduced volume thermal conductivity detector, Anal. Chem. 45 (13) (1973) 2191–2198.
[36] S. Sorge, et al., Fully integrated thermal conductivity sensor for gas chromatography without dead volume, Sens. Actuators A: Phys. 63 (3) (1997) 191–195.
[37] W. Kuipers, et al., Sensitivity of a planar micro-flame ionization detector, Talanta 82 (5) (2010) 1674–1679.
[38] M. Moorman, et al., Microcombustor array and micro-flame ionization detector for hydrocarbon detection, in: Proc. SPIE – MEMS Components and Applications for Industry, Automobiles, Aerospace, and Communication II, San Jose, CA, USA, 2003, pp. 40–50.
[39] Z. Ouyang, et al., Miniature mass spectrometers, Annu. Rev. Anal. Chem. 2 (1) (2009) 187–214.
[40] J.C.T. Eijkel, et al., A dc microplasma on a chip employed as an optical emission detector for gas chromatography, Anal. Chem. 72 (11) (2000) 2547–2552.
[41] B. Mitra, et al., The micromachined flashFET: a low-power, three-terminal device for high speed detection of vapors at atmospheric pressure, in: 18th IEEE International Conference on Micro Electro Mechanical Systems, 2005. MEMS, 2005, pp. 794–797.
[42] B. Mitra, et al., The detection of chemical vapors in air using optical emission spectroscopy of pulsed microdischarges from two- and three-electrode microstructures, Sens. J. IEEE 8 (8) (2008) 1445–1454.
[43] Y.-M. Fu, et al., Characteristic responses of an atmospheric pressure DC micro-plasma detector for gas chromatography to organic functional groups, Microchem. J. 89 (1) (2008) 7–12.
[44] S. Narayanan, et al., A micro-discharge photoionization detector for micro-gas chromatography, Microchim. Acta 1–7 (2013).
[45] R.P. Manginell, et al., Diagnostic potential of the pulsed discharged helium ionization detector (PDHID) for pathogenic mycobacterial volatile biomarkers, J. Breath Res. 7 (3) (2013) 037107.
[46] W.E. Wentworth, et al., Pulsed discharge photoionization detector: application to analysis of chloro alkanes/alkenes, J. High Resolut. Chromatogr. 19 (2) (1996) 85–90.
[47] D.S. Forsyth, Pulsed discharge detector: theory and applications, J. Chromatogr. A 1050 (1) (2004) 63–68.
[48] S. Narayanan, et al., Fabrication and characterization of a suspended TCD integrated with a gas separation column, J. Microelectromech. Syst. 22 (5) (2013) 1166–1173.

Biographies

Shree Narayanan holds a PhD in electrical engineering from Virginia Polytechnic Institute and State University (Virginia Tech), Blacksburg, VA, USA. His doctoral research at the VTEMS Laboratory, Virgina Tech, focused on the development of innovative gas detectors that can be monolithically integrated with gas chromatography separation columns without loss of sensitivity. He has a MS from the same department, for his thesis on the impedance measurement of biological cells. Prior to joining Virginia Tech, he finished his Bachelors in electronics and communication engineering from PES Institute of Technology, Bangalore, India.

Gary Rice received his BS degree in chemistry from James Madison University in 1976 and PhD in analytical chemistry from Iowa State University in 1981. He was a postdoctoral research associate at the Ames National Laboratory in Ames, IA from 1981 until 1984 when he joined the chemistry faculty at the College of William and Mary in Williamsburg, VA. In addition to serving as chair of the department from 2001 to 2009, he has received awards from both the Alumni Association and the College for sustained excellence in teaching. His research interests span a broad range of analytical applications, including environmental analysis, analytical atomic spectroscopy, and chromatographic processes and development.

Masoud Agah received his BS and MS degrees in electrical engineering from Sharif University of Technology (SUT), Iran, in 1996 and 1998, respectively, and his PhD degree from the University of Michigan, Ann Arbor, in 2005. He began his undergraduate studies in 1992 after being awarded by the President of Iran for achieving the first rank in the Nationwide Iranian University Entrance Examination. During his studies, he received numerous awards, including the Iranian Exemplary Graduate Student Honor, awarded by President Khatami in 1998. In 2000, he joined the NSF Center for Wireless Integrated MicroSystems (WIMS ERC), University of Michigan, where he developed MEMS-based gas chromatography columns for environmental monitoring applications. He joined the faculty of Virginia Tech in August 2005, where he is currently an associate professor in the Bradley Department of Electrical and Computer Engineering with a courtesy appointment in the Department of Mechanical Engineering. He is also a core faculty member of Virginia Tech-Wake Forest School of Biomedical Engineering and Sciences. He established the VT MEMS Laboratory in 2005 and has focused his research on environmental and biomedical applications of MEMS and nanotechnology. He is a senior member of the Institute of Electrical and Electronic Engineers (IEEE) and a member of the American Society for Mechanical Engineers (ASME).